Journal of Power Sources 196 (2011) 1061–1068

Contents lists available at ScienceDirect

Journal of Power Sources

journal homepage: www.elsevier.com/locate/jpowsour

Nafion-based composite electrolytes for proton exchange membrane fuel cells operating above 120 °C with titania nanoparticles and nanotubes as fillers

B.R. Matos[a], E.I. Santiago[a], J.F.Q. Rey[b], A.S. Ferlauto[c], E. Traversa[d,e], M. Linardi[a], F.C. Fonseca[a,*]

[a] Instituto de Pesquisas Energéticas e Nucleares, São Paulo, SP 05508-000, Brazil
[b] Universidade Federal do ABC, Santo André, SP 09210170, Brazil
[c] Departamento de Física, Universidade Federal de Minas Gerais, Belo Horizonte, MG 31270-901, Brazil
[d] University of Rome Tor Vergata, 00133 Rome, Italy
[e] International Center for Materials Nanoarchitectonics (MANA), National Institute for Materials Science, Tsukuba 305-0044, Ibaraki, Japan

ARTICLE INFO

Article history:
Received 29 June 2010
Received in revised form 6 August 2010
Accepted 9 August 2010
Available online 18 August 2010

Keywords:
Nafion
Composite
PEM fuel cell
Titania
Nanotubes

ABSTRACT

Nafion/titania-based fillers composites are prepared by casting and tested in proton exchange membrane fuel cells (PEMFCs) operating at elevated temperatures (130 °C). Three types of titania-based fillers are studied: nanoparticles with nearly spherical shape, mesoporous particles with high surface area, and hydrogen titanate nanotubes. Properties of composites related to PEMFC operation, such as water absorption/retention and proton conductivity, are determined and correlated with microstructural data obtained by small-angle X-ray scattering. The addition of titanate nanotubes changes more markedly the physical properties of the composite electrolytes as compared to titanium oxide nanoparticles with different surface area, a feature probably related to the intrinsic hydration and proton conductivity of the nanotubes. Polarization curves of H_2/O_2 PEMFCs using composite electrolytes indicate that composite electrolytes contribute to a significant boost of H_2/O_2 PEMFC performance at 130 °C.

1. Introduction

There is a great interest to boost proton exchange membrane fuel cell (PEMFC) performance at operation temperatures above 80 °C [1,2]. Although PEMFCs are considered very promising for clean and efficient electric power generation, increasing their operation temperature could improve performance by overcoming several issues. The electrochemical properties that govern the PEMFC performance, such as electrode reaction kinetics and ion transport, are thermally activated and could be greatly enhanced with a temperature increase of ~50 °C with respect to the usual operation temperature (~80 °C). In addition, increased operation temperature is believed to contribute to a better thermal and water management of the PEMFC system, and to an enhanced tolerance to fuel contaminants, such as carbon monoxide [1].

However, the increase in the PEMFC operation temperature above 80 °C with Nafion, the most used polymeric electrolyte, has not been achieved [3]. In fact, Nafion becomes an insulator when water is not present to promote proton dissociation from sulfonic acid groups; hence, at temperatures above 80 °C, water evaporation increases drastically the electrolyte ohmic resistance [3]. Such a restriction has motivated great research efforts and the increase in the PEMFC operating temperature is considered as one of the most important step to advance this technology towards commercialization [4–7].

It is possible to identify two main research strategies for the development of PEMFC electrolytes for high temperature operation: (i) electrolytes capable of operating at elevated temperatures without the need of hydration, such as polybenzimidazole (PBI) and Nafion imidazole composites [5,6]; and (ii) electrolytes capable of water retention at elevated temperatures [7]. The later approach involves basically the replacement of Nafion by a Nafion/ceramic composite [8]. The inorganic (ceramic) fillers consist of hydrophilic nanoparticles with high surface area that should increase the water retention capacity of the electrolyte by providing a high fraction of structurally adsorbed water. Additionally, other positive characteristics have been found in Nafion/ceramic composites, such as enhanced thermomechanical properties [9–11] and decreased fuel crossover in direct alcohol fuel cells (DAFCs) [12].

A consistent correlation between the properties of Nafion/ceramic composites and the PEMFC performance is directly linked with the understanding of Nafion microstructural properties [13,14]. Nafion structure is made up of a nanometric scale mixture of hydrophobic and hydrophilic phases. The hydrophobic backbone is semi-crystalline and confers to Nafion good mechanical properties [15]. The hydrophilic phase forms ionic clusters, which percolate upon hydration, forming an interconnected structure that

* Corresponding author. Tel.: +55 11 31339282; fax: +55 11 31339285.
E-mail address: fcfonseca@ipen.br (F.C. Fonseca).

0378-7753/$ – see front matter © 2010 Elsevier B.V. All rights reserved.
doi:10.1016/j.jpowsour.2010.08.025

Table 1
General properties of titania-based fillers.

Particle	Crystalline phase	Surface specific area ($m^2\ g^{-1}$)	Particle mean diameter (nm)	Pore mean diameter (nm)
TiO_2 P25 Degussa TP25	80% anatase, 20% rutile	50	25	–
TiO_2 mesoporous TMP	anatase	115	5–20	3.5
Nanotube TNT	$H_2Ti_3O_7$	150	7–10	3.5[a]

[a] Nanotube inner diameter.

is responsible for the excellent proton conduction exhibited by Nafion electrolytes [13,14].

Composite electrolytes with the addition of different ceramic phases, such as TiO_2, SiO_2, ZrO_2, and Al_2O_3 have been investigated [16,17]. In the case of DAFCs, the use of Nafion/ceramic composites resulted in enhanced performance, and a systematic dependence on both the specific surface area and the acid character of the particles has been observed [17]. High surface area particles with an acid character, such as SiO_2 and TiO_2, were found to result in better fuel cell performance when compared to other oxides [17]. On the other hand, the performance of hydrogen fueled PEMFCs using composite membranes displays less evident dependence on the composition, volume fraction, and surface acidity of the oxide phase [9,16]. Such a different behavior of composites when used in PEMFCs or DAFCs has generated distinct interpretations concerning the role played by the inorganic phase [17,18]. Most of the reported results have indicated that the water retention on high surface area oxide particles at elevated temperature is the predominant effect for the improved performance of PEMFCs [4,8]. However, due to the complex nature of the Nafion structure [13] and possible intricate interactions between the polymer and the oxide particles, resulting from both the surface properties of the ceramics and the preparation methods of the composites, a clear understanding of the effects of the oxide particle addition on the PEMFC properties is still a matter of discussion [16,19].

In the present study, titania-based particles with different morphologies were studied as fillers in cast Nafion membranes. Titania-based materials were selected due to their hygroscopic properties and availability in different microstructures and crystallographic phases, including mesoporous anatase nanoparticles or hydrogen titanate nanotubes, which exhibit properties such as high surface area and proton conductivity [20]. The fabricated composites were characterized in detail regarding the main physical properties related to PEMFC operation, such as water absorption/retention and proton conductivity, which were correlated with structural data obtained by small-angle X-ray scattering. Finally, the composite electrolytes were tested for operation in H_2/O_2 PEMFC up to 130 °C.

2. Experimental

2.1. Titania-based fillers

Three types of titania-based materials were used to fabricate Nafion-based composite electrolytes: commercial Degussa (now Evonik) P25 titania (TP25), mesoporous anatase (TMP), and hydrogen titanate nanotubes (TNT). Further details on the preparation of the TMP and TNT powders are described elsewhere [20,21]. Table 1 displays the main microstructural properties of the studied particles.

2.2. Preparation of the composite membranes

Electrolyte composites were prepared by the casting method. Nafion 5% solution (Dupont) was evaporated at 80 °C and redissolved in dimethylsulfoxide (DMSO – Aldrich). The resulting solution was kept under stirring for 24 h at room temperature. Separately, the desired amount of titania-based fillers (TP25, TMP, or TNT) was dispersed in DMSO under mechanical stirring for 24 h at room temperature. The Nafion-DMSO solution and the titania-based dispersion were added together and kept under stirring for 24 h, followed by an ultrasonic bath for 1 h. The homogenized mixture was dispensed in an aluminum mold for evaporation in a resistive furnace at 160 °C. Composite membranes were prepared with the addition of inorganic phase concentrations $x = 2.5$, 5.0, 10, and 15 wt.%. Cast Nafion ($x = 0$ wt.%) membranes (Ncast) were produced by following the described procedure, and commercial Nafion 115 (Dupont) membrane was used as a reference for some measurements.

The fabricated membranes were post-treated in three different solutions: HNO_3 (7 mol L^{-1}), H_2O_2 (3 vol.%), and H_2SO_4 (0.5 mol L^{-1}) at 80 °C for 1 h, with intermediate washing steps with deionized water for organic solvent residues removal and to assure the protonic (H^+) form of the polymeric matrix. The final thickness of membranes was 105 ± 5 μm.

2.3. Characterization of Nafion/titania-based membranes

The water uptake of cast membranes, defined as $\Delta m\ (\%) = (m_S - m_D)/m_D$, was evaluated by weighing the dry membrane (m_D), after thermal treatment at 110 °C for 3 h, and the water saturated membrane (m_S) after boiling in water for 1 h.

The mass loss dependence on the temperature of water saturated samples was evaluated by thermogravimetric (TG) analysis (Setaram-LabSys) carried out in the temperature range of 25–140 °C using a heating rate of 5 °C min^{-1} under Ar flow (40 mL min^{-1}). Then, the system was cooled down to room temperature at 20 °C min^{-1} and a second TG run was performed up to 250 °C, under the same conditions of the first heating, to analyze the mass loss of dried samples.

Small-angle X-ray scattering (SAXS) experiments were carried out using synchrotron radiation at the SAXS beamline of the Brazilian National Synchrotron Light Laboratory (LNLS). Experiments were conducted with an incident wavelength $\lambda = 1.488$ Å in the range of the scattering vector $q \sim 0.02$–0.35 $Å^{-1}$ ($q = 4\pi \sin\theta/\lambda$, being 2θ the scattering angle). Small-angle X-ray scattering patterns from all the samples were collected with MarCCD detector and the intensity curves were corrected for parasitic scattering, integral intensity, and sample absorption. SAXS measurements of hydrated samples were carried out after immersing the membranes in deionized water for 24 h. For samples with known water content the measurements were carried out with Kapton envelopes, which covered both membrane faces to prevent water evaporation. Different degrees of water content were obtained by controlling the time in which the hydrated membranes were exposed to air. The membrane water content was determined gravimetrically, as previously described.

The proton conductivity of the membranes was measured by impedance spectroscopy (IS) using a frequency response analyzer (Solartron 1260) and a homemade Teflon sample holder with in-plane Pt terminal leads and a K-type thermocouple. The sample holder was inserted in a closed flask containing water to ensure RH 98% during measurements. Two-probe IS measurements were performed in the 25–80 °C temperature range, in the 100 Hz to 1 MHz frequency interval, with 200 mV applied amplitude.

2.4. Preparation and characterization of PEMFCs

Membrane electrode assemblies (MEAs), with 5 cm^2 area, were fabricated by hot pressing electrodes to the cast membranes at 125 °C and 1000 kgf cm^{-2} for 2 min. The detailed preparation of gas diffusion electrodes and MEAs has been described elsewhere [22].

The polarization curves (*I–V*) were taken at different temperatures by progressively heating the system from 80 °C up to 130 °C. For each measuring temperature, the system was stabilized and conditioned by draining electrical current at a fixed voltage of 0.7 V for 2 h before data collection in order to reach steady state. For measurements at 80 °C, the reactant gases, O_2 and H_2, were water saturated by passing them through humidifiers at 85 and 95 °C, respectively. For higher temperatures (from 100 to 130 °C), humidifiers were set at the same temperature of the cell. All experiments were performed under an absolute pressure of 3 bar to ensure 100% of relative humidity (RH). For some selected concentrations, two membranes were produced for checking the reproducibility of the *I–V* results. In addition, the stability of the composite electrolytes was evaluated by performing *I–V* measurements of the single cells at 80 and 130 °C after consecutive heating/cooling cycles between these two temperatures.

3. Results and discussion

3.1. Composite characterization

The water uptake (Δm) of Nafion (Ncast and Nafion 115) and composites TP25 (Degussa P25), TMP (mesoporous titania), and TNT (titanate nanotubes) is shown as a function of particle concentration in Fig. 1. The water uptake of Ncast ($x = 0$ wt.%) was $\Delta m = 42\%$, a value larger than that of Nafion 115 ($\Delta m = 34\%$). The fabrication process of extruded Nafion 115 results in an oriented structure that can inhibit the polymer swelling [13]. The addition of TP25 and TMP titania particles slightly decreased the water uptake of cast membranes, and the composites with the highest oxide content studied ($x = 15$ wt.%) had $\Delta m \sim 35\%$. On the other hand, the addition of TNT resulted in a marked increase of water absorption, reaching $\Delta m \sim 60\%$ for the sample with $x = 15$ wt.% [23]. Although part of the enhanced water absorption can be attributed to the large surface area of TNT, such a difference cannot be accounted only to structural properties of the studied particles and it is possibly correlated with the physicochemical properties of the titanate nanotubes. The higher water absorption of TNT composite can be attributed to both the nanotubular structure of titanates and to the

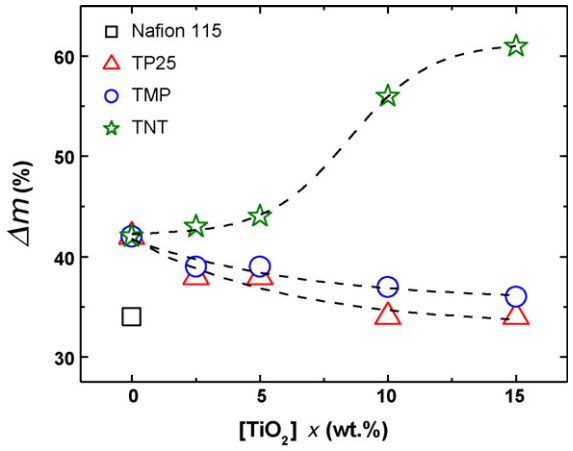

Fig. 1. Water uptake, measured at room temperature, for Nafion 115, Nafion cast, and Nafion/titania-based composites as a function of the inorganic phase concentration.

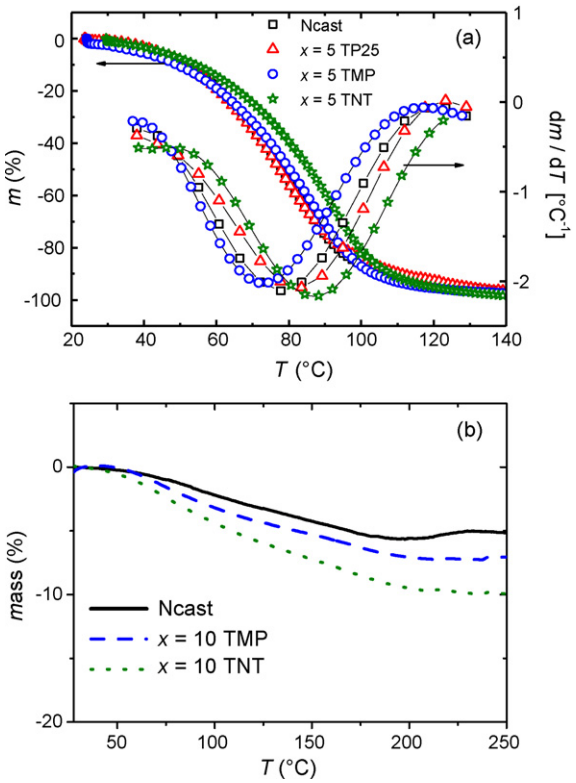

Fig. 2. (a) Mass loss of water saturated Nafion cast ($x = 0$ wt.%) and composites with $x = 5.0$ wt.% of TMP, TP25, and TNT (left *y*-axis). Each curve was normalized by the net mass loss between 20 and 140 °C. Temperature dependence of the derivative of thermogravimetric curves (right *y*-axis). (b) Mass loss of Nafion and composites TNT and TMP with $x = 10$ wt.%, previously dried at 150 °C in dry Ar atmosphere.

large amount of water molecules that can be present in the TNT [20]. The structure of titanate nanotubes was reported to be a stacking of lamellar TiO_6 octahedra intercalated with alkali cations or protons [24]. In the protonic form, such a structure stores water in different configurations, either as crystallographic or physically adsorbed molecules [25]. In addition, several types of protons, present either as ion exchangeable hydroxyl groups or absorbed water confers to TNT an acid surface and high water storage capacity [25].

Along with the water uptake, the water retention of the electrolyte at high temperature is an important parameter for high temperature PEMFC application. Fig. 2a shows the normalized thermogravimetric (TG) curves of water saturated cast composites (left *y*-axis) and the correspondent derivative (right *y*-axis). The observed mass loss can be attributed to the release of weakly bond water absorbed in the membrane. For all studied samples, the onset of water release was ~45 °C and the mass loss was completed at $T \sim 130$ °C. The derivative curves (right axis) exhibited a minimum that indicates the temperature of maximum water loss rate. For cast Nafion such a minimum was at ~80 °C, a value ~10% lower than the one for Nafion 115 (not shown) [26]. Although cast Nafion has higher water absorption than Nafion 115 (Fig. 1), the absorbed water evaporates at lower temperatures, a feature probably related to the microstructural differences resulting from the fabrication processes of the membranes.

The composites ($x = 5$ wt.%) exhibited TG derivative minima at 90, 83, and 74 °C for TNT, TP25, and TMP, respectively. The derivative curves of the TP25 and TMP composites and the Ncast are similar, indicating that addition of titania particles, with surface specific area of ~50 $m^2\,g^{-1}$ (TP25) and ~100 $m^2\,g^{-1}$ (TMP), does not result in significant increases in the water retention capacity of Nafion. On the other hand, the composites with TNT showed

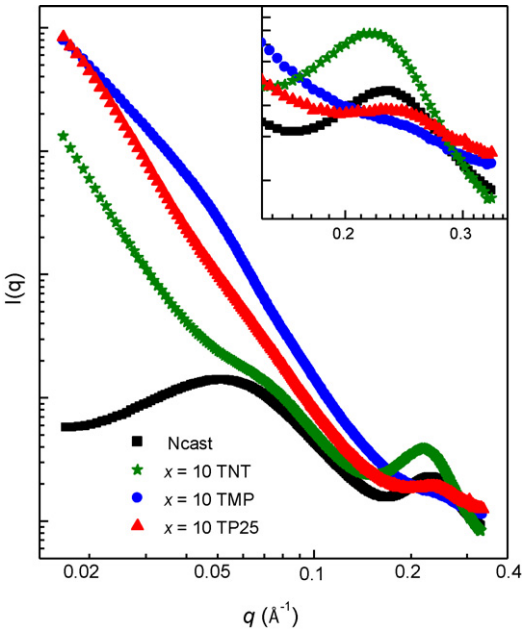

Fig. 3. Small-angle X-ray scattering patterns of the TP25, TMP, and TNT dry composites.

increased water retention that can be related to its structural properties.

The water retention was further evaluated by a second TG run of previously analyzed samples, as shown in Fig. 2b. The total mass loss up to 250 °C was ~5, 7, and 10% for Nafion, TMP, and TNT composites, respectively, clearly indicating that the inorganic fillers contribute to the water retention at high temperature. Such losses were much lower than the ones of water saturated samples (Fig. 2a), and can be associated with the release of molecular bonded water. It has been reported that composite electrolytes with the addition of mesoporous titania enhanced PEM fuel cell performance, attributed to increased water absorption by capillary condensation in the mesoporous structure [27,28]. However, the combined effect of mesoporosity, physically adsorbed water, and hydroxyl groups on the titanate nanotubes can contribute for a more effective water retention, as exhibited by composites with TNT [25,29].

Fig. 3 shows small-angle X-ray scattering (SAXS) curves for dry samples of Ncast, and of composites (x = 10 wt.%) with TMP, TP25, and TNT. The scattering pattern of Nafion shows two characteristic peaks corresponding to ionic clusters (hydrophilic clusters) and to crystallites of the hydrophobic backbone at $q \sim 0.23$ Å^{-1} and ~0.07 Å^{-1}, respectively, in good agreement with literature data [30,31]. In the SAXS pattern of the composite with TNT, the ionic cluster peak of Nafion is slightly displaced to lower q values, possibly due to some residual absorbed water. An abrupt increase of the scattered intensity in the low-q range ($q < 0.04$ Å^{-1}) indicates the presence of agglomerated nanotubes located outside the ionic cluster, but no clear evidence of a characteristic correlation length could be inferred. Composites with TP25 and TMP showed more convoluted SAXS patterns, which were attributed to larger scattering of the inorganic particles. Nevertheless, it can be observed that the position of the peak corresponding to the ionic clusters is barely affected by the addition of the TMP or TP25 phases (see inset of Fig. 3), indicating that Nafion structure is not significantly changed. A careful inspection of SAXS data revealed that both TP25 and TMP patterns display a slender shoulder at low $q \sim 0.022$ Å^{-1} and 0.042 Å^{-1}, respectively, which can be associated with the scattering of agglomerated particles. The correlation lengths attributed to such scatterings are 28 and 15 nm, respectively, in good agreement with the dimensions of both TP25 and TMP particles listed in Table 1. The evidence of particle agglomeration, inferred from SAXS analyses, suggests that composite membranes have microstructure similar to other cast composite reported previously, which showed a concentration gradient of titania across the membrane [32].

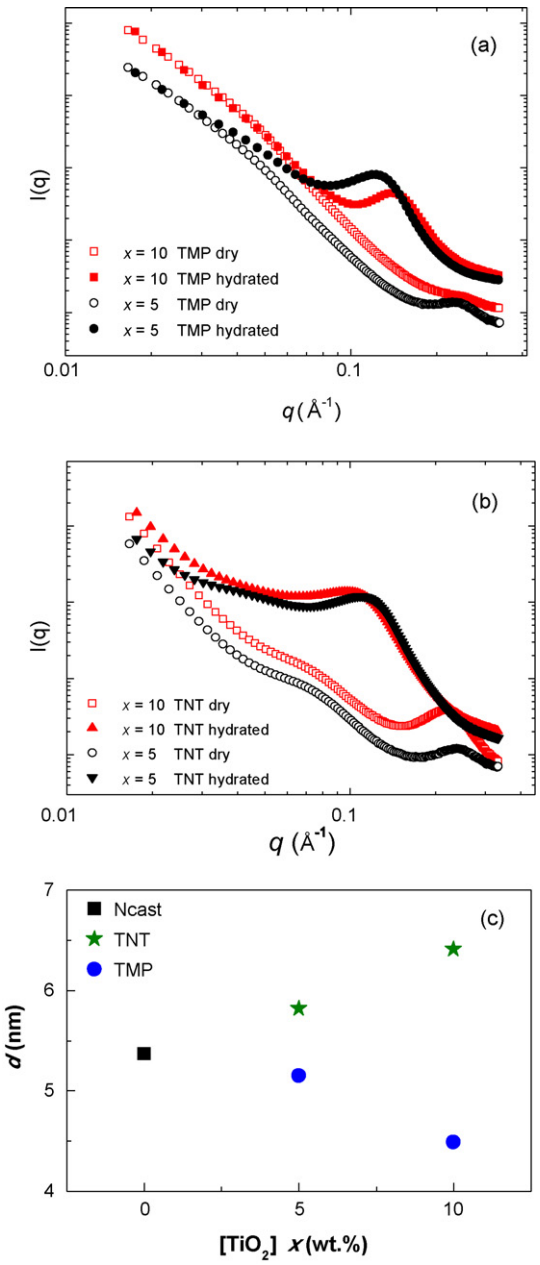

Fig. 4. Small-angle X-ray scattering patterns of composites TMP (a) and TNT (b) with x = 5 and 10 wt.% in both dry and fully hydrated conditions. (c) Coherence length of fully hydrated conditions as a function of the inorganic phase concentration.

The effect of both hydration and inorganic particle concentration was also evaluated by SAXS analysis. Fig. 4a and b show SAXS data of TMP and TNT composite samples with x = 5 and 10 wt.% in dried and fully hydrated states. It is observed that the position of the ionic cluster peak is strongly dependent on the water content and the displacement of the peak position from the hydrated ($q \sim 0.10$ Å^{-1}) to the dried ($q \sim 0.23$ Å^{-1}) condition is within the range observed for Nafion [31,33]. The coherence lengths $d = 2\pi/q$, associated with the ionic clusters, can be related to the ionic cluster size and were calculated from SAXS data and shown in Fig. 4c. In dried conditions, both composites exhibited similar cluster size,

$d \sim 2.5$ nm. However, upon hydration, interesting features can be observed in the dependence of d on the inorganic phase content. Upon hydration of composites, the increase in TMP concentration (from 5 to 10 wt.%) resulted in a smaller size of the ionic cluster (4.5 nm). On the contrary, the increase in TNT concentration to 10 wt.% resulted in a more pronounced peak displacement towards low q values, reflected by an increased size of ionic clusters (6.4 nm). As inferred from SAXS data, TMP composites displayed a shift of the peak position compatible with a less expanding microstructure, while TNT composites showed that increasing fraction of the titanate nanotubes increased the expansion of the ionic clusters and improved the membrane water absorption; in perfect accordance with the water uptake data (Fig. 1).

The analysis of the SAXS results allowed the gathering of several features related to the structure of the studied composites. Firstly, the phase-separated structure of the polymeric matrix is practically unchanged by the addition of the inorganic fillers, as inferred from the analysis of dry membranes [30,31]. Based on the particle sizes, displayed in Table 1, and the characteristic dimensions of ionic clusters, obtained from the results of SAXS analysis, it is reasonable to assume that the titania-based particles are located outside the ionic clusters and exhibit some agglomeration. Nonetheless, the ionomer peak displacement upon hydration suggests that the inorganic particles influence the ionic cluster arrangement of Nafion upon hydration. Even though inorganic particles are likely to be located outside the ionic clusters, SAXS data suggest possible interactions between inorganic and organic phases that depend on the intrinsic properties of the particles. Titania nanoparticles probably act as pinning centers that constrain the polymeric structure, as previously inferred from differential calorimetric data that showed higher glass transition temperature for TMP composites than for Nafion [16,26]. Markedly, titanate nanotubes, possibly due to the large number of water molecules and ion exchangeable protons on the nanotube surface, are prone to interact with the Nafion matrix allowing for higher expansion of the ionic clusters and favoring a higher water uptake.

The measured electrical properties of the composite electrolytes can be directly correlated with the microstructural features previously discussed. Fig. 5 shows the Arrhenius plots for the TP25 (Fig. 5a), TMP (Fig. 5b), and TNT (Fig. 5c) composites. For all composites, the ionic conductivity [$\sigma(T)$] exhibited a thermally activated Arrhenius-type behavior within the temperature range investigated. The calculated activation energy for proton conduction for Ncast was ~0.1 eV, in good agreement with previous findings [34]. The activation energy of the composite membranes was essentially the same of Nafion, suggesting that the proton transport mechanism was not modified by the incorporation of titania-based particles. This result is in agreement with the SAXS analysis, which demonstrated that the ionic network structure of Nafion is preserved in composite samples.

The addition of inorganic phases, even though it did not affect proton transport mechanisms, resulted in a reduction in proton conductivity values. For low concentrations ($x \leq 10$ wt.%), a rather weak dependence of $\sigma(T)$ on weight fraction was observed, while a more significant drop in conductivity was observed for TP25 and TMP composites for $x \geq 10$ wt.%. Samples with $x = 15$ wt.% showed for TP25 and TMP composites $\sigma(80\,^{\circ}\mathrm{C}) = 0.14$ and $0.11\,\mathrm{S\,cm^{-1}}$, respectively. Such behavior can be explained by percolation theory. TP25 and TMP particles act as insulating phases added to the conducting Nafion matrix, resulting in a progressive decrease in conductivity with increasing the particle concentration.

On the other hand, TNT composites showed a much less pronounced decrease in $\sigma(T)$ with increasing x, and for $x = 15$ wt.%, $\sigma(80\,^{\circ}\mathrm{C}) = 0.17\,\mathrm{S\,cm^{-1}}$, which corresponds to ~85% of the $\sigma(80\,^{\circ}\mathrm{C})$ of Nafion. In fact, it has been reported that hydrated hydrogen titanate nanotubes exhibit high proton conductivity in the

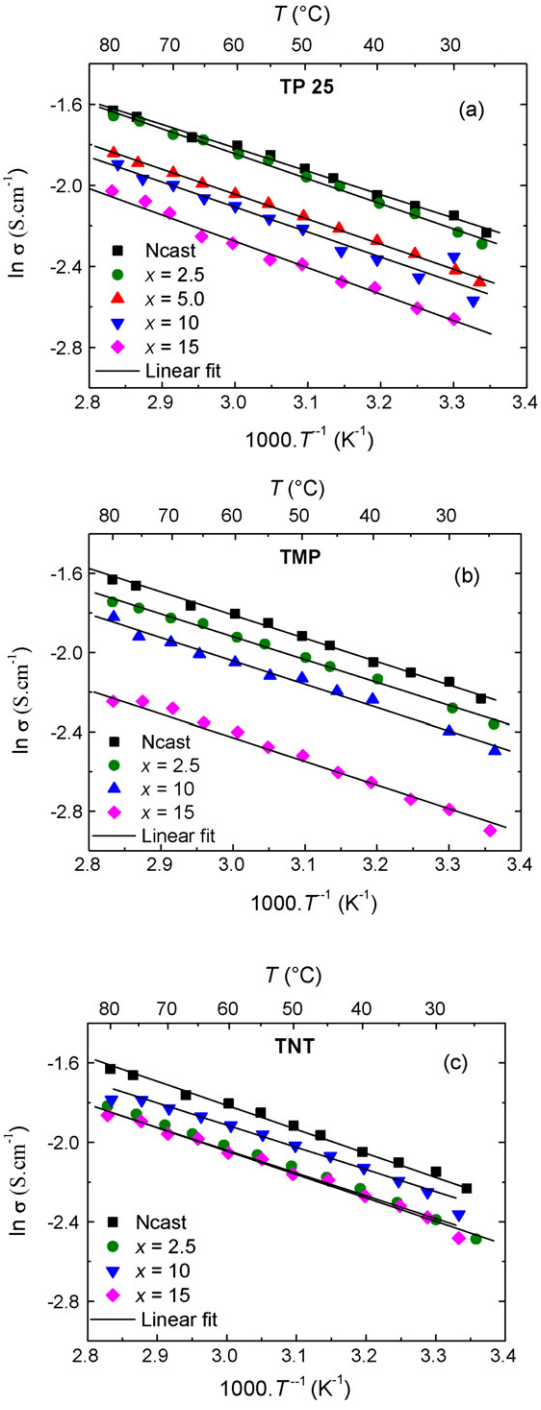

Fig. 5. Arrhenius plots of composite electrolytes (a) TP25, (b) TMP, and (c) TNT measured at RH = 98%.

50–160 °C temperature range, presenting transport mechanism and activation energy values similar to Nafion [29]. Therefore, in the case of TNT composites, the lower decrease in σ is possibly related to the intrinsic proton conductivity of titanate nanotubes and increased water retention/absorption of the TNT composites [20].

3.2. Fuel cell tests

To evaluate the PEMFC performance of composite electrolytes operating at high temperature, polarization (I–V) curves were taken at different temperatures. Fig. 6 shows the polarization curves of fuel cells operating at 80 and 130 °C using the TP25, TMP, and TNT

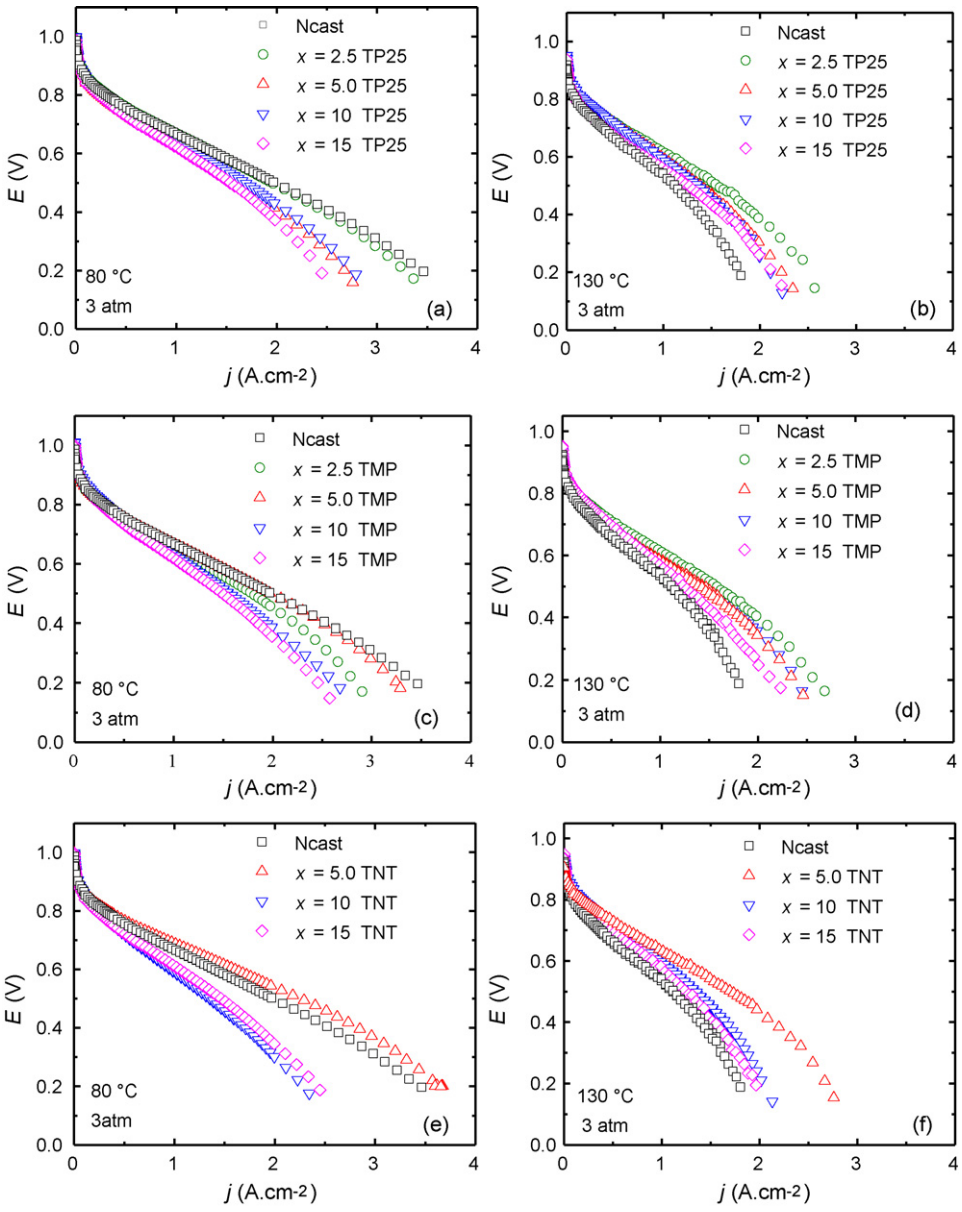

Fig. 6. Polarization (*I–V*) curves for the (a, b) TP25, (c, d) TMP, and (e, f) TNT composites measured at 80 and 130 °C.

composite electrolytes. *I–V* curves measured at 80 °C exhibited a gradual loss of performance with increasing the filler concentration in the electrolytes. Such an effect is more discernible in the linear region on the polarization curve and is associated with ohmic losses within the electrolyte, a result consistent with the measured decrease in ionic conductivity with increasing the inorganic phase content (Fig. 5). On the other hand, at 130 °C the performance of fuel cells using composite electrolytes exceeded the performance of cast Nafion. The experimental results showed that at the higher temperature Nafion exhibited a marked loss of performance, while composite electrolytes practically sustained at 130 °C the same current density measured at 80 °C. Furthermore, TNT composites ($x = 5$ wt.%) displayed a noticeable increase in performance both at low and high temperatures, and a more detailed discussion was presented elsewhere [23].

The main differences in the *I–V* curves can be attributed to the ohmic drop region that is associated with the transport properties of the electrolytes. Thus, the area specific conductivity (*S*) was calculated from the linear portion at intermediate current densities. To better compare the performance of fuel cells with different electrolytes, Fig. 7 shows the temperature dependence of both *S* (Fig. 7a) and the current density (*j*) at 600 mV (Fig. 7b) for composites with selected concentrations. The general behavior in both panels of Fig. 7 indicated that fuel cell performance is directly correlated to the conductivity of the electrolytes. Upon heating, *S* displayed a slight increase up to ~110 °C and a fast decrease with further temperature increase, but composite samples had a much less pronounced drop of *S* than cast Nafion. The TNT composite with $x = 5$ wt.% had the highest specific conductivity over the entire temperature range, and at $T > 120$ °C all composite samples with $x < 15$ wt.% exhibited specific conductivity higher than cast Nafion. Accordingly, as inferred from *j* (Fig. 7b), it was observed that the performance of fuel cells also increased when the temperature was raised from ~80 to ~100 °C. With further temperature increase (>100 °C), cast Nafion showed a pronounced performance loss, while composite electrolytes exhibited a much less temperature-dependent current density. Above 110 °C, the composites practically sustained the performance at 80 °C, which represents a noticeable gain of current density at high temperatures.

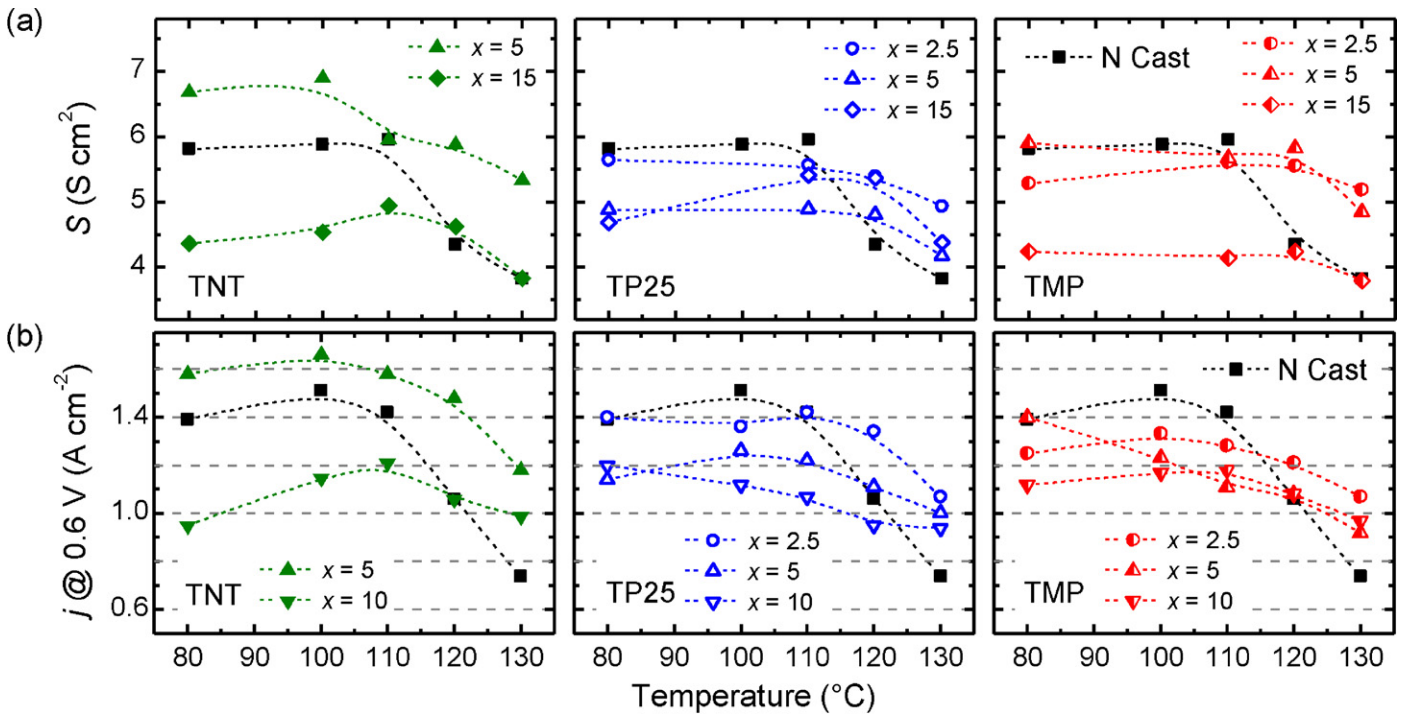

Fig. 7. (a) Temperature dependence of the area specific conductivity calculated from polarization curves for selected compositions of composite electrolytes. (b) Current density j at 600 mV as a function of the temperature for the samples with $x = 0$, 2.5, 5.0 and 10 wt.% of TP25, TMP, and TNT.

Interestingly, the TNT composite with $x = 5.0$ wt.% exhibited the best performance in the entire temperature range tested. At 130 °C, TNT composite with $x = 5$ wt.%, and both TMP and TP25 composites with $x = 2.5$ wt.% showed current densities that represent an enhancement of ~60% and 45%, respectively, in comparison to Nafion. In addition, samples with $x = 10$ wt.% have current densities of ~1 A cm^{-2} at 130 °C, a value 25% higher than the one of cast Nafion. Such values demonstrate that composite electrolytes

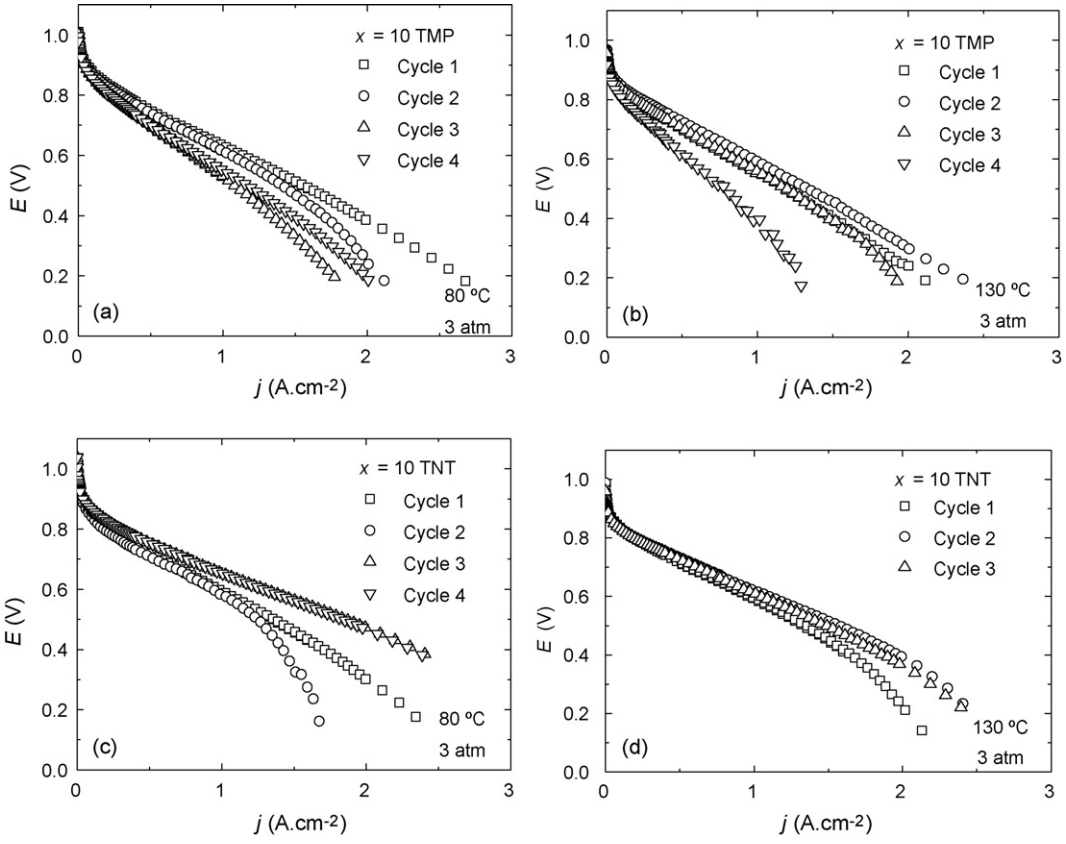

Fig. 8. Polarization (I–V) curves as a function of the successive cycles measured at 80 and 130 °C.

have superior performance at high temperature that depends on both the concentration and properties of titania-based fillers. For TNT, a proton-conducting filler, the best performance was achieved at $x = 5.0$ wt.%, whereas more insulating fillers exhibit best performance at lower concentrations of inorganic particles ($x = 2.5$ wt.%). Such different optimal concentrations reflect a balance between low-ohmic losses and enhanced water retention in PEM fuel cells operating at high temperature provided by titania-based fillers.

Fig. 8 displays *I–V* results of fuel cells using TNT and TMP composite electrolytes measured during sequential heating/cooling cycles between 80 and 130 °C. Such harsh conditions promote thermal stress and provide an indication of the applicability of the studied fuel cells rather than an more elaborated measurement protocol to access membranes stability. The main changes observed between cycles were in the high current density region of *I–V* curves and are likely to be related to diffusion processes occurring at the electrodes. In Fig. 8a, *I–V* curves of the cell with the TMP composite evidenced a fast degradation after subsequent temperature cycles. On the other hand, the cell with the TNT composite showed a better stability. Above 110 °C, Nafion loses structural stability due to the evaporation of bulk water inside the membrane. Such a thermal stress can promote shrinkage of the polymer that hinders the Nafion capacity to reabsorb water and to achieve its previous performance, when the temperature is reduced back to 80 °C [35–37]. The good stability displayed by the Nafion-TNT composite after the thermal cycles indicated that water adsorption and retention play a significant role in maintaining hydration at elevated temperatures and, consequently, in diminishing thermal stress of the membrane.

4. Conclusions

A detailed characterization of cast Nafion/titania-based composites evidenced that the water absorption/retention capacity of the inorganic phase plays an important role on both the structural and electrical properties of the composite electrolytes. Titania nanoparticles did not change significantly the water absorption/retention of composite electrolytes. However, the addition of hydrogen titanate nanotubes, a proton-conducting phase with both high surface area and high water retention capacity, was found to significantly enhance the properties of composite electrolytes without decreasing considerably the proton conductivity. Such features contributed to a significant boost of H_2/O_2 PEMFC performance and enhanced stability at 130 °C.

Acknowledgments

The authors are thankful to FAPESP, CNPq (BRM, ML, ASF, FCF), FAPEMIG, CAPES, FINEP, CNEN, and Laboratório Nacional de Luz Síncrotron (LNLS) under the Project Number 5150.

References

[1] Y. Shao, G. Yin, Z. Wang, Y. Gao, J. Power Sources 167 (2007) 235–242.
[2] S. Licoccia, E. Traversa, J. Power Sources 159 (2006) 12–20.
[3] P.C. Rieke, N.E. Vanderborgh, J. Membr. Sci. 32 (1987) 313–328.
[4] G. Alberti, M. Casciola, Annu. Rev. Mater. Res. 33 (2003) 129–154.
[5] K.D. Kreuer, J. Membr. Sci. 185 (2001) 29–39.
[6] Y.-Z. Fu, A. Manthiram, J. Electrochem. Soc. 154 (2007) B8–B12.
[7] J.A. Kerres, J. Membr. Sci. 185 (2001) 3–27.
[8] V. Baglio, A.D. Blasi, A.S. Aricò, V. Antonucci, P.L. Antonucci, C. Trakanprapai, V. Esposito, S. Licoccia, E. Traversa, J. Electrochem. Soc. 152 (2005) A1373–A1377.
[9] M.B. Satterfield, P.W. Majsztrik, H. Ota, J.B. Benziger, A.B. Bocarsly, J. Polym. Sci. Part B. Polym. Phys. 44 (2006) 2327–3235.
[10] S.K. Young, K.A. Mauritz, J. Polym. Sci. Part B Polym. Phys. 39 (2001) 1282–1295.
[11] V. Di Noto, R. Gliubizzi, E. Negro, G. Pace, J. Phys. Chem. B 110 (2006) 2497–2501.
[12] Y.S. Park, Y. Yamazaki, Eur. Polym. J. 42 (2006) 375–388.
[13] K.A. Mauritz, R.B. Moore, Chem. Rev. 104 (2004) 4535–4586.
[14] K. Schmdit-Rohr, Q. Chen, Nat. Mater. 7 (2008) 75–83.
[15] H.W. Starkweather, Macromolecules 15 (1982) 320–323.
[16] K.T. Adjemian, R. Dominey, L. Krishnan, H. Ota, P. Majsztrik, T. Zhang, J. Mann, B. Kirby, L. Gatto, M. Velo-Simpson, J. Leahy, S. Srinivasan, J.B. Benziger, A.B. Bocarsly, Chem. Mater. 18 (2006) 2238–2248.
[17] V. Baglio, A.S. Aricò, A. Di Blasi, V. Antonucci, P.L. Antonucci, S. Liccocia, E. Traversa, S.R. Fiory, Electrochim. Acta 50 (2005) 1241–1246.
[18] E. Chalkova, M.B. Pague, M.V. Fedkin, D.J. Wesolowski, S.N. Lvov, J. Electrochem. Soc. 152 (2005) A1035–A1040.
[19] D. Truffier-Boutry, A. De Geyer, L. Guetaz, O. Diat, G. Gebel, Macromolecules 40 (2007) 8259–8264.
[20] T. Kasuga, Thin Solid Films 496 (2006) 141–145.
[21] C. Trakanprapai, V. Esposito, S. Licoccia, E. Traversa, J. Mater. Res. 20 (2005) 124–128.
[22] V.A. Paganin, E.A. Ticianelli, E.R. Gonzales, J. Appl. Electrochem. 26 (1996) 297–304.
[23] B.R. Matos, E.I. Santiago, F.C. Fonseca, M. Linardi, V. Lavayen, R.G. Lacerda, L.O. Ladeira, A.S. Ferlauto, J. Electrochem. Soc. 154 (2007) B1358–B1361.
[24] E. Morgado Jr., P.M. Jardim, B.A. Marinkovic, F.C. Rizzo, M.A.S. de Abreu, J.L. Zotin, A.S. Araújo, Nanotechnology 18 (2007) 495710.
[25] D.V. Bavykin, M. Carravetta, A.N. Kulak, F.C. Walsh, Chem. Mater. 22 (2010) 2458–2465.
[26] B.R. Matos, E.M. Aricó, M. Linardi, A.S. Ferlauto, E.I. Santiago, F.C. Fonseca, J. Therm. Anal. Calorim. 97 (2009) 591–594.
[27] S.Y. Chen, C.C. Han, C.H. Tsai, J. Huang, Y.W. Chen-Yang, J. Power Sources 171 (2007) 363–372.
[28] K.R. Payer, K.D. Hammond, G.A. Tompsett, L. Krough, M.N. Pratt, W.C. Conner Jr., J. Porous Mater. 16 (2009) 91–99.
[29] M. Yamada, M. Wei, I. Honma, H. Zhou, Electrochem. Commun. 8 (2006) 1549–1552.
[30] T.D. Gierke, G.E. Munn, F.C. Wilson, J. Polym. Sci. Polym. Phys. Ed. 19 (1981) 1687–1704.
[31] G. Gebel, Polymer 41 (2000) 5829–5838.
[32] E. Chalkova, M.V. Fedkin, D.J. Wesolowski, S.N. Lvov, J. Electrochem. Soc. 152 (2005) A1742–A1747.
[33] M. Fujimura, T. Hashimoto, H. Hawai, Macromolecules 15 (1982) 136–144.
[34] R.C.T. Slade, J. Barker, Solid State Ionics 35 (1989) 11–15.
[35] G. Gebel, P. Aldebert, M. Pineri, Macromolecules 20 (1987) 1425–1428.
[36] L.M. Onishi, J.M. Prausnitz, J. Newman, J. Phys. Chem. B 111 (2007) 10166–10173.
[37] R.S. Yeo, J. Electrochem. Soc. 130 (1983) 533–538.